Design and Optimization of Hydrofoils tailored for Marine Current Turbines

Francisco Espenica
francisco.espenica@tecnico.ulisboa.pt

Instituto Superior Técnico, Universidade de Lisboa, Portugal

November 2018

Abstract

The design and optimization of hydrofoils tailored for marine current turbines is considered. For the definition of operating conditions, a reference turbine is designed using a lifting line theory based routine, with blades integrating hydrofoils of series NACA 63-8XX. The designed turbine yields an improvement of 10% when compared to previous works in turbine lifting line predictions. The influence of N_{crit} factor on hydrofoil performance and angle of attack is studied, resulting in the use of value 4 to mimic operating conditions. An analytical methodology to calculate the influence of shear flow, difference in depth, yaw misalignment and rotor pre-bend on angle of attack and effective velocity is implemented. This analytical methodology is used to determine the operational envelope of each turbine blade section. For hydrofoil optimization, an already existing multi-objective optimization through genetic algorithm framework is used. Cost functions are developed with the objectives of maximizing lift to drag ratio and lift coefficient for free and forced transition and maximizing cavitation margin for each hydrofoil and blade section. Optimized hydrofoils IST-MT1-XX are obtained, yielding improvements in lift to drag ratio and lift coefficient for both regimes up to 73.21% and 99.82% respectively, for the same cavitation performance as reference hydrofoils, while also yielding cavitation margins of up to 3, relative to the local cavitation number. Finally, the reference turbine is redesigned to incorporate the optimized hydrofoils and tested with the same lifting line routine, yielding an improvement of 0.33% in power coefficient for the same design conditions and reducing blade chord up to 41%.

Keywords: Hydrofoil, turbine, multi-objective, optimization, cavitation

1. Introduction

Worldwide energy consumption has been continuously growing year after year due to increasing global population and technological development. This increased consumption has been supported throughout the years mainly by fossil-fuels and other non renewable sources, which are widely known as being non-sustainable in the long haul and harmful to the environment. With environmental and sustainability concerns in mind and due to the limitations of currently industrialized sources of renewable energy, research has been conducted in recent years in the area of ocean energy. Cumulative ocean energy installed capacity has doubled worldwide from less than 12 MW in 2016 to over 25 MW in 2017, according to the OES (Ocean Energy Systems) annual report [1].

Many types of energy can be extracted from the ocean, such as thermal, ocean osmosis (salinity gradients), biomass, wave energy (power harnessed from wind driven waves) and hydro-kinetic energy (extraction of kinetic energy from current motion), being the last two the main focus of recent research [2]. Among these, hydro-kinetic energy extraction from currents generated by tidal motion is more advantageous due to the high predictability of its source. The horizontal-axis current turbine (HACT) appears to be the most technologically and economically viable hydro-kinetic energy harnessing technology currently available [3][4].

Although there are many similarities between wind turbines and horizontal axis marine current turbines, or HAMCTs, the latter pose different problems and engineering challenges due to the harsh environment in which they operate. Among these, one can point out corrosion of blades and nacelle [5], marine fouling [6] and scour on seabed (which can lead to structure instability) [7].

One major concern regarding marine current turbines is cavitation on blades, which can, depending on its extent and severity, cause breakdown of turbine operation, blade surface erosion, noise and structural vibrations [8]. In particular, cavitation erosion can damage the turbine blades by removing

the protective coating, exposing the blade shell to aggressive marine environment, followed by gradual damage to the blade material.
With these considerations in mind, this work seeks to develop a hydrofoil design procedure employing an already existing foil optimization framework [9]. Cost functions are developed in order to characterize and maximize hydrofoil performance and lower the risk of cavitation. Finally, a reference turbine is redesigned incorporating the optimized hydrofoils and checked for overall improved performance.

Previous works on this area include those of Ouyang *et.al* [10], in which a numerical procedure for the optimization of a two-dimensional hydrofoil is developed; the foil shape is parametrized by Bezier curves, and the optimization is performed using a genetic algorithm under three objective functions that translate into enhanced performance regarding lift and drag. Goundar *et.al* [11] obtained a profile named HF-Sx for the outer half span of a turbine blade that outperforms previous designs in the literature. This hydrofoil is based on the standard S1210 with a 20% increase in camber and thickness and numerically and experimentally studied. Xing-Qi *et.al* [12] proposes a multipoint optimization method in which foil shapes are parametrized by Bezier curves and the optimization is carried out by the NSGA-II genetic algorithm. The hydrofoil's characteristics are obtained through computational fluid dynamics, CFD, simulation. The optimization effort focuses on enhancing the performance of the NACA 63-815 for lift to drag ratio and cavitation performance; in general, improvements of more than 10% are obtained. Sacher *et.al* [13] uses a surrogate-based optimization that substitutes the objective function of the problem by a model constructed from a limited number of computations at selected design points. This procedure is applied to the design of the shape and the elastic characteristics of a hydrofoil equipped with deformable elements providing flexibility to the trailing edge. The optimization concerns the minimization of the hydrofoil drag while ensuring a non-cavitating flow, at selected sailing conditions.

2. Reference turbine definition

The definition of a reference turbine is needed to characterize the operating conditions to which the blade sections are be subjected to, namely, Reynolds number, effective inflow speed, V_{eff}, and cavitation number, σ. The reference turbine is designed based on work published by Bahaj *et.al* [14]. As such, the blade sections of the reference turbine are composed by hydrofoils of series NACA 63-8XX. The reference turbine is designed using a computer routine based on lifting line theory, developed at Instituto Superior Técnico, in Lisbon, Portugal [15].

2.1. N_{crit} factor influence on hydrofoil performance

The parameter N_{crit} is the exponent in the e^n method and is a user-specified value in XFOIL. N_{crit} is the logarithm of the amplification factor of the most-amplified frequency which triggers transition. The value of this parameter depends on the ambient disturbance level in which the foil operates, and mimics the effect of such disturbances on transition [16]. The change of this value is studied regarding its influence on hydrofoil NACA 63-815 performance for various relevant Reynolds numbers.

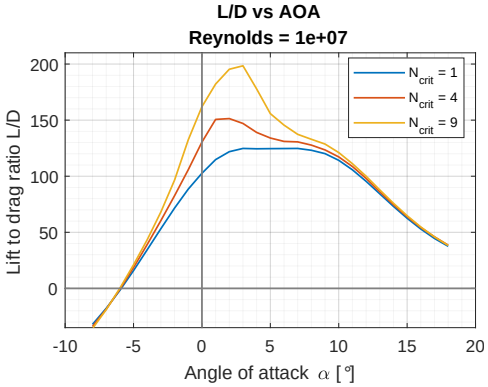

Figure 1: N_{crit} influence on L/D vs AOA for Reynolds number of $1{\cdot}10^7$

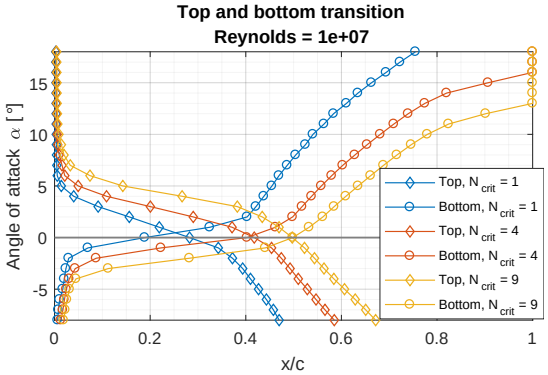

Figure 2: N_{crit} influence on the transition location on the upper and lower foil surfaces for Reynolds number of $1{\cdot}10^7$

There is a significant loss of performance as factor N_{crit} is reduced from 9 to 1 (figure 1), as well as a change in the optimum angle of attack. Also, transition occurs earlier for all angles of attack as N_{crit} decreases (figure 2). In light of these results, $N_{crit} = 4$ is considered an appropriate value for "mimicking" the operating conditions.

2.2. Reference turbine characteristics and performance

Table 1 specifies the reference turbine project characteristics. The design TSR is 6 and the rated flow speed U_0 is 2 m/s. Figures 3 and 4 display the

turbines chord and pitch, respectively. Figure 5 displays a comparison of C_P vs TSR of different results: lifting line results of the full scale reference turbine; lifting line results of the Bahaj model turbine [17] and experimental data of the same turbine [14]. It is possible to observe that the reference turbine has a higher C_P of 0.4833 than lifting line predictions made for the Bahaj turbine, $C_P = 0.4393$. Also, maximum C_P occurs at different TSR.

Table 1: Turbine physical dimensions and flow characteristics

Variable		Value
Hub height to sea floor h_0	m	15
Hub depth to sea level d_0	m	15
Diameter D	m	20
Number of blades	-	3
Fluid density ρ	kg/m^3	1025
Fluid vapour pressure p_v	Pa	1670
Fluid kinematic viscosity ν	m^2/s	$1.18{\cdot}10^{-6}$
Rated flow speed U_0	m/s	2
Design tip speed ratio TSR	-	6

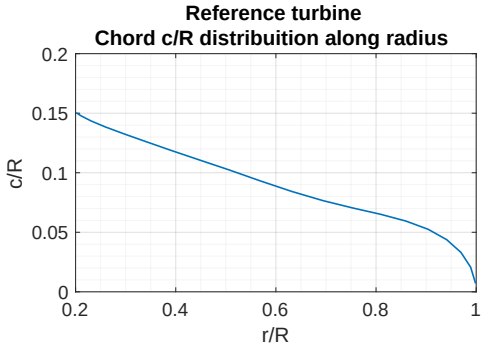

Figure 3: Chord distribution

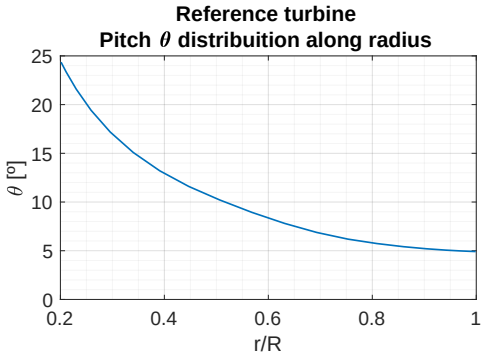

Figure 4: Pitch distribution

Figure 6 displays the operating curves (cavitation number vs angle of attack AOA along blade radial sections) of the reference turbine. These curves are obtained with an analytical method [18] which takes into account the influence of shear flow, difference in depth, yaw misalignment and rotor pre-bend on angle of attack and effective velocity estimation. Each curve in fig. 6 represents the variation of AOA and cavitation number σ felt at that r/R for half of a complete rotor revolution.

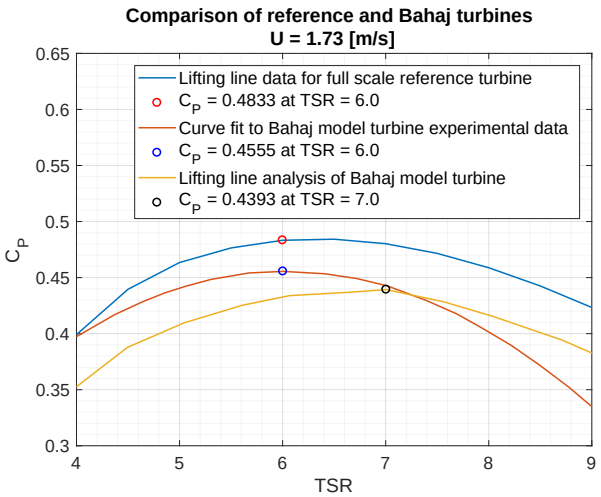

Figure 5: Reference full scale turbine lifting line data, Bahaj curve fit to experimental data of model turbine [14] and lifting line predictions of Bahaj model turbine [17].

$$\sigma = \frac{p_\infty - p_v}{1/2 \cdot \rho {V_{eff}}^2} \tag{1}$$

Cavitation number is calculated through eq. 1, where V_{eff} is the effective flow velocity at the section.

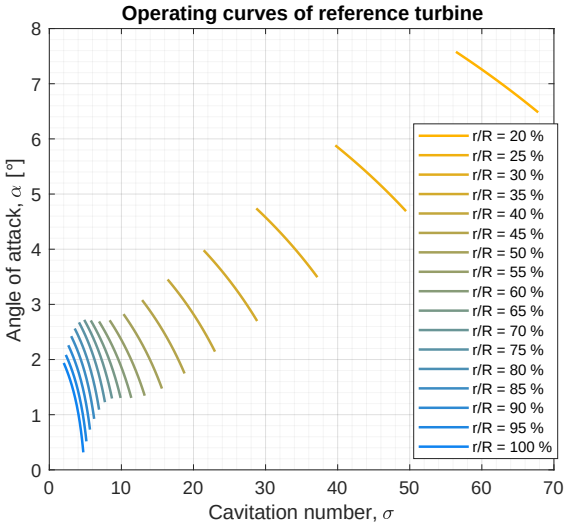

Figure 6: Operating curves of blade sections along the span - cavitation number vs AOA at section

For simplicity, the designed reference turbine does not have pre-bend on its blades and there is no yaw misalignment with the flow.

3. Cost function development and optimization framework

The optimization routine used for this work relies on the mathematical description of the foil shape with CST parametrization [19] and the NSGA-II

multi-objective optimization algorithm to render optimal compromises between design goals. For more detailed information the reader is referred to [9] and [20]. The genetic algorithm considers 100 foil candidates per generation and each simulation considers 50 generations. Two specific hydrofoil performance cost functions, CFs, are defined as design goals. CF1, relates to hydrodynamic performance, contrasting with CF2, cavitation performance. Cavitation performance is defined as increasing the margin between cavitation number σ and the minimum pressure coefficient $C_{p_{min}}$ of the hydrofoil. Each optimized hydrofoil has a unique score when considering a specific cost function. These scores are displayed in a Pareto front, which is composed by the set of design CF scores that are Pareto efficient (see figure 7). Each point in the Pareto front represents an optimized hydrofoil.

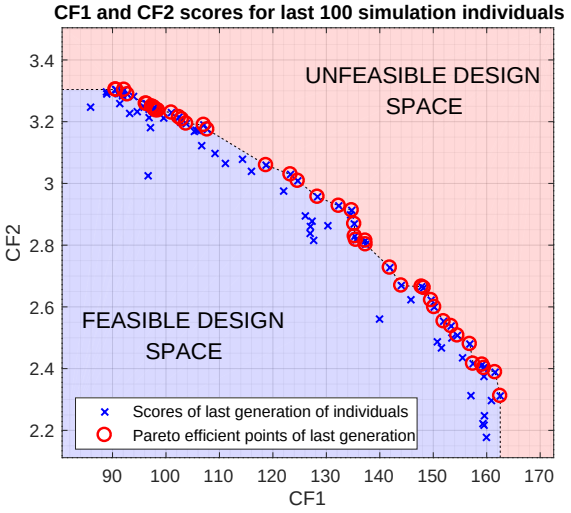

Figure 7: Pareto efficient points in last generation of a simulation

The optimization is carried out for specific sections of the blade and outputs hydrofoils with predefined maximum relative thickness (see table 2).

Table 2: Reference turbine data

Span r/R [%]	Chord c/R [%]	Thickness t/c [%]	Pitch θ [°]	Reynolds Re [-]
20	15.0	24.0	24.4	3.9e+06
30	14.4	21.0	21.6	4.1e+06
45	11.1	18.0	11.6	5.3e+06
75	5.9	15.0	5.4	5.3e+06
100	0.7	12.0	4.9	7.2e+05

3.1. Cost function 2, CF2

CF2 is calculated as follows:

$$CF2 = \sigma_{min}^{r/R} - (-C_{p_{min}})_{max} \tag{2}$$

$\sigma_{min}^{r/R}$ is calculated with eq. 1; it corresponds to the minimal cavitation number of each operation curve (see figure 6), for each section of the turbine blades. $(-C_{p_{min}})_{max}$ corresponds to the minimum C_p value found within the range of operating angles of attack of the hydrofoil at the section, meaning:

- The AOA_{opt} is the AOA at which the foil exhibits the highest L/D value ;
- C_p distribution around the foil is calculated for angles of attack ranging between $AOA_{opt} - {}^{\Delta\alpha}/_{2} \rightarrow AOA_{opt} + {}^{\Delta\alpha}/_{2}$, where $\Delta\alpha$ is the variation in angle of attack experienced at the section (see figure 6) ;
- The minimum value of $C_{p_{min}}$ for this whole range, which corresponds to $(-C_{p_{min}})_{max}$, is taken.

3.2. Cost function 1, CF1

The performance of each candidate hydrofoil is obtained with free transition (no prescribed transition location) and forced transition (trip located at x/c = 10% of the lower surface and 5% of the upper surface of the hydrofoil [21]). The final version of CF1 considers both regimes and is calculated as follows:

$$w_1 = w_2 = 0.25 \qquad w_0 = 0.5 \tag{3}$$

$$\begin{aligned} AOA_i &= AOA_{opt} \\ AOA_{i-j} &= AOA_{opt} - {}^{\Delta\alpha}/_{2} \\ AOA_{i+j} &= AOA_{opt} + {}^{\Delta\alpha}/_{2} \end{aligned} \tag{4}$$

$$\begin{aligned} C_L^{weighted} &= w_1 \cdot C_L\,|_{AOA_{i-j}} \\ &+ w_0 \cdot C_L\,|_{AOA_i} + w_2 \cdot C_L\,|_{AOA_{i+j}} \end{aligned} \tag{5}$$

$$\begin{aligned} L/D^{weighted} &= w_1 \cdot L/D\,|_{AOA_{i-j}} \\ &+ w_0 \cdot L/D|_{AOA_i} + w_2 \cdot L/D|_{AOA_{i+j}} \end{aligned} \tag{6}$$

$$n = number\ of\ reference\ hydrofoils$$

$$C_L^{ref} = \frac{\sum_{n=1}^{n} 1.1 \cdot C_{L\,n}^{weighted}}{n} \tag{7}$$

$$L/D^{ref} = \frac{\sum_{n=1}^{n} 1.1 \cdot L/D_n^{weighted}}{n} \tag{8}$$

$$C_{L\,new\,foil}^{adim} = \left(\frac{C_{L\,new\,foil}^{weighted} - C_L^{ref}}{C_L^{ref}} + 1 \right)^2 \tag{9}$$

$$L/D_{new\,foil}^{adim} = \left(\frac{L/D_{new\,foil}^{weighted} - L/D^{ref}}{L/D^{ref}} + 1 \right)^2 \tag{10}$$

$$\begin{aligned} CF1 &= 0.5 \cdot \left[C_{L\,new\,foil}^{adim} + L/D_{new\,foil}^{adim} \right]_{free} \\ &+ 0.5 \cdot \left[C_{L\,new\,foil}^{adim} + L/D_{new\,foil}^{adim} \right]_{forced} \end{aligned} \tag{11}$$

$C_L^{weighted}$ $(L/D^{weighted})$ are values which are calculated (see eqs. 5 and 6) by making a weighted

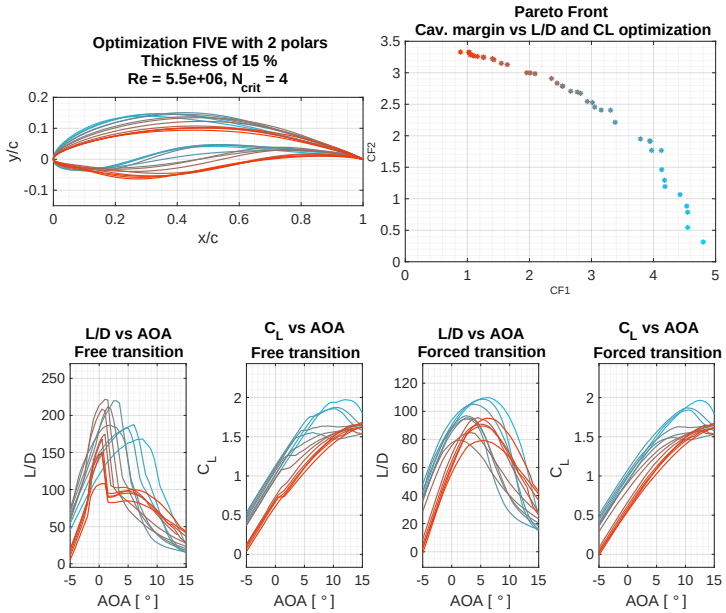

Figure 8: Foils geometry, Pareto front and L/D obtained with CF1 FIVE C

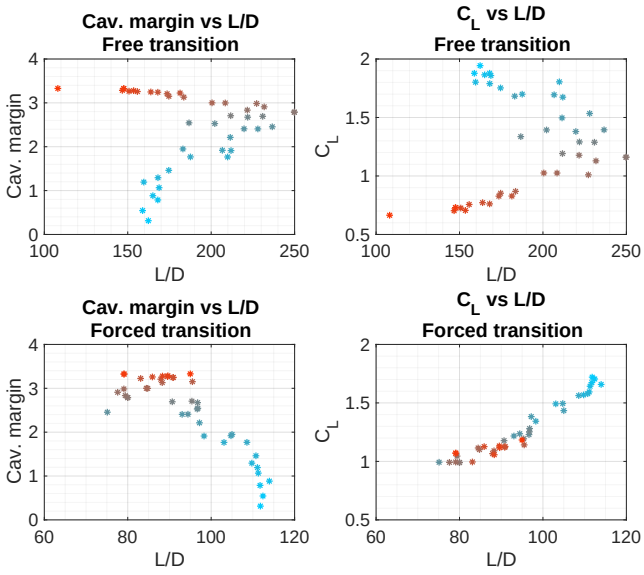

Figure 9: Version FIVE C of CF1 - Comparison of free and forced transition regimes with various distributions

sum of C_L (L/D) over a range of angles of attack defined by eqs. 4, considering the relative weights of eq. 3 . Eqs. 7 and 8 calculate the mean value of $C_L^{weighted}$ and $L/D^{weighted}$ between the reference hydrofoils considered (NACA 63-8XX and 66-8XX series). Through eqs. 9 and 10, $C_L^{weighted}$ and $L/D^{weighted}$ of the new hydrofoil are directly compared to reference values. The square factor directs the optimization routine to further improve the value of CF1 to the detriment of CF2. Finally, the value of CF1 is calculated through eq. 11. This formulation intends to improve performance with both free and forced transition. This type of optimization is termed C, and its objective is to obtain hydrofoils that have a balanced performance between clean (free transition) and rough (forced transition) regimes. This CF yields the results present in figures 8 and 9 for t/c_{max} of 15%.

4. Hydrofoil design results

Optimization FIVE C yields the results on figures 10 and 11 for $t/c_{max} = 24\%$. Figure 12 contains a direct comparison of optimized hydrofoils with the respective reference hydrofoils. CF1 and CF2 scores are calculated for the reference hydrofoils, which allows for a direct comparison. Regarding hydrofoil NACA 63-824, the optimized hydrofoil with the same cavitation margin shows increases of 73.21% and 99.82% in maximum L/D and C_L, respectively, for the rough regime. The same optimized hydrofoil improves the clean regime performance by 4.81% in maximum L/D and 4.01% in optimum C_L.

Optimization FIVE C is carried out for all sections and thicknesses displayed in table 2.
Because the section at $r/R \approx 100\%$ is the most prone to cavitation, additional optimizations are

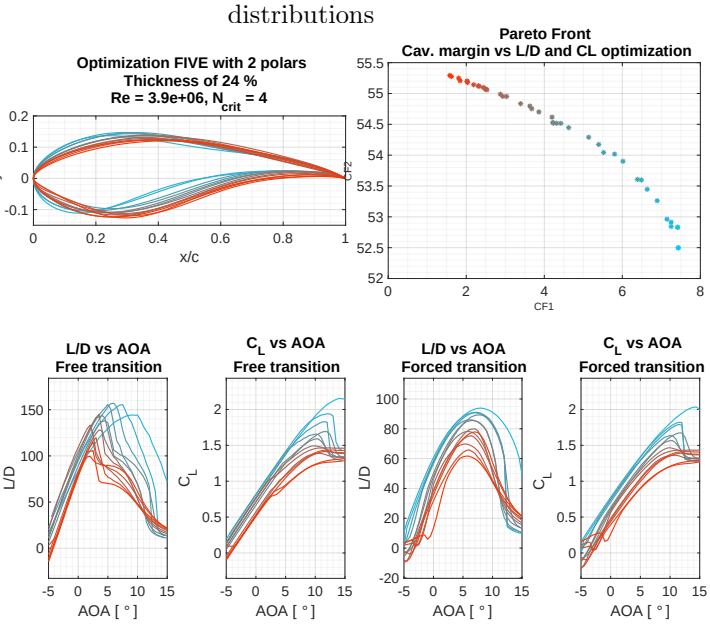

Figure 10: Foils, Pareto front and L/D obtained with CF1 FIVE C for hydrofoils of thickness $t/c = 24\%$

made in order to further improve the performance of the 12% thickness hydrofoil, while not losing cavitation performance. CF1 version EIGHT C (see eqs. 12, 13 and 14) is used, yielding the results shown in figures 13, 14.

$$C_{L\,new\,foil}^{adim} = \left(\frac{C_{L\,new\,foil}^{weighted} - C_L^{ref}}{C_L^{ref}} + 1 \right)^3 \qquad (12)$$

$$L/D_{new\,foil}^{adim} = \left(\frac{L/D_{new\,foil}^{weighted} - L/D^{ref}}{L/D^{ref}} + 1 \right)^3 \qquad (13)$$

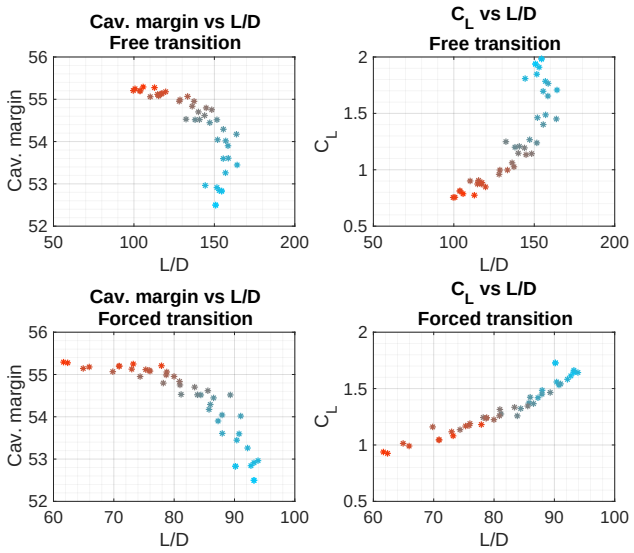

Figure 11: Thickness of 24% - Comparison of free and forced transition regimes

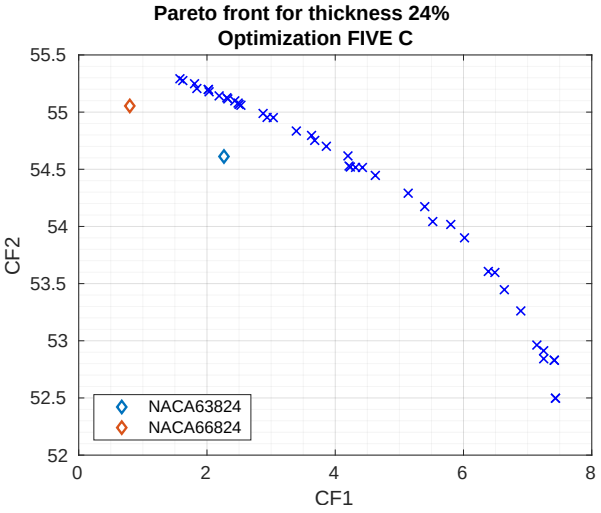

Figure 12: Thickness of 24% - Comparison with reference hydrofoils, thickness of 24%

$$CF2 = \left(\left(\sigma_{min}^{r/R} - (-C_{p_{min}})_{max}\right) + 1\right)^3 \qquad (14)$$

This formulation successfully increased values of L/D for both regimes with a small reduction in cavitation margin.

For this optimization one of the reference hydrofoils is S1210. Optimization results show 6 novel foils that outperform S1210, all having greater cavitation margin (see figure 15). The first optimized hydrofoil (greater CF1 value in fig. 15) improves the performance of S1210 by 12.63% and 11.56% in maximum L/D and optimum C_L, respectively, in clean regime. In rough regime there is a decrease of 2.17% in L/D and an increase of 3.03% in optimum C_L.

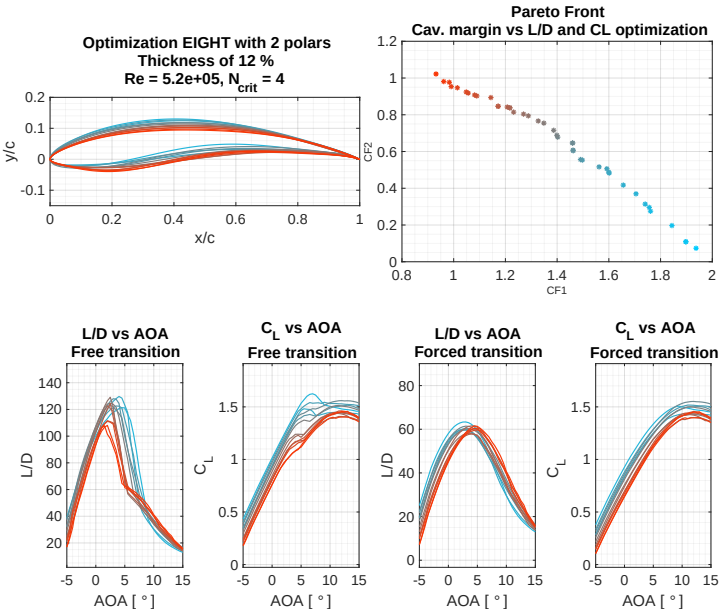

Figure 13: Foils, Pareto front and L/D obtained with CF1 FIVE C for hydrofoils of thickness $t/c = 12\%$

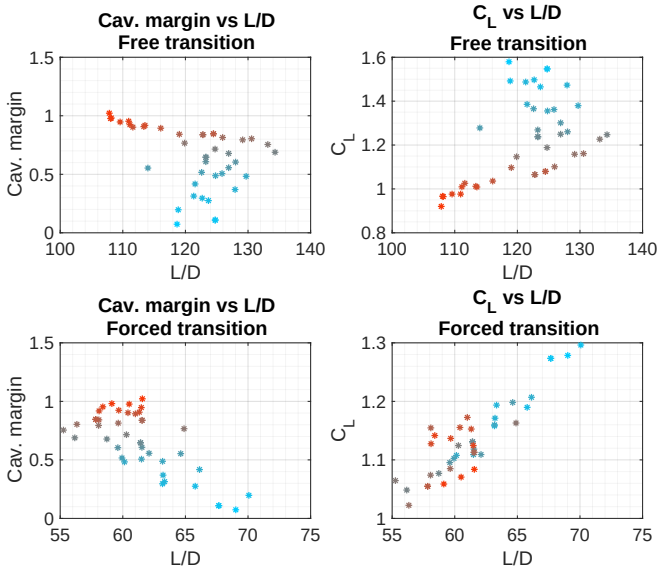

Figure 14: Thickness of 12%, optimization FIVE C - Comparison of free and forced transition regimes

4.1. Selected hydrofoils

Five hydrofoils are chosen, one for each blade section. IST-MT1-XX is the name chosen for the hydrofoils, and stands for:

- IST - **I**nstituto **S**uperior **T**écnico, faculty in which this work is produced ;
- MT1 - **M**arine **T**urbine, generation of hydrofoils **1**, i.e., first hydrofoils produced by a work of this type ;
- XX - Two numbers denoting the maximum thickness of the hydrofoil. If maximum t/c is 18%, the foil is named IST-MT1-18.

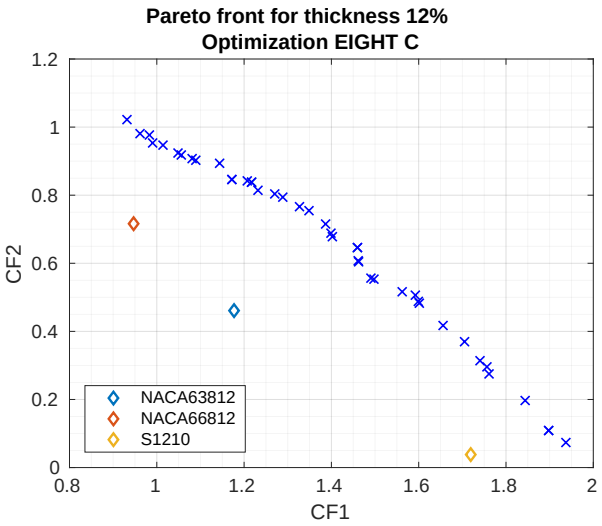

Figure 15: Thickness of 12% - Comparison with reference hydrofoils

The criteria of selection for the hydrofoils are as follows:

- Equal or similar optimum angle of attack between adjacent sections of the blade ;
- High value of L/D, in order to obtain a greater energy conversion efficiency in turbine operation, translated in a higher value of power coefficient C_P. In this hydrofoils selection, emphasis is given to L/D in the clean regime ;
- Similarity of the hydrofoil geometry along the radius of the blade r, according to common practice [22].

Cavitation margin is also taken into account in the selection of each hydrofoil. Figure 16 displays hydrofoils chosen for all sections, along with relevant data.

5. Redesigned turbine

The reference turbine is redesigned through the lifting line routine to incorporate the optimized hydrofoils IST-MT1-XX. Figures 17 and 18 display the obtained chord and pitch, respectively. Figure 19 contains a comparison of the reference turbine and novel turbine C_P vs TSR distribution. An improvement of 0.33% is obtained in design conditions, while an increase of 1.16% is obtained when comparing at TSR of 6.5.
The redesigned turbine displays a smaller chord than the reference turbine, which suggests that the same power output with much smaller chord is achievable with a turbine that incorporates hydrofoils IST-MT1-XX. A chord reduction of up to 41% is obtained. Table 4 displays redesigned turbine data and figure displays the blade layout.

Table 3: Blade section information

Span r/R [%]	Foil at section	Reynolds Re [-]
20	IST-MT1-24	3.3e+06
30	IST-MT1-21	3.1e+06
45	IST-MT1-18	3.1e+06
75	IST-MT1-15	3.8e+06
100	IST-MT1-12	6e+05

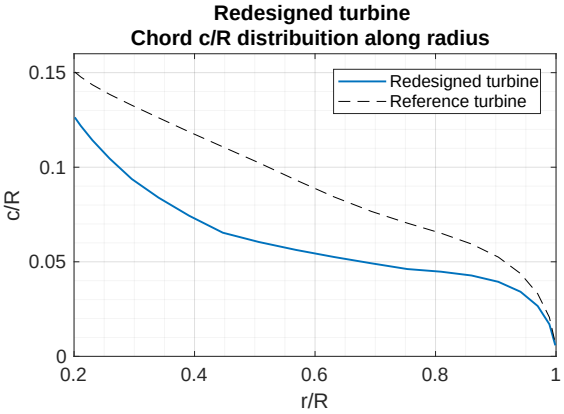

Figure 17: Chord distribution

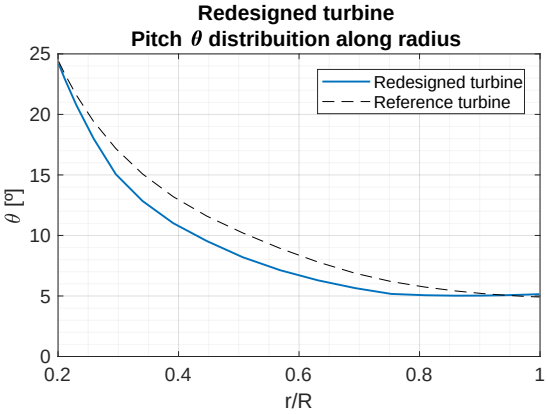

Figure 18: Pitch distribution

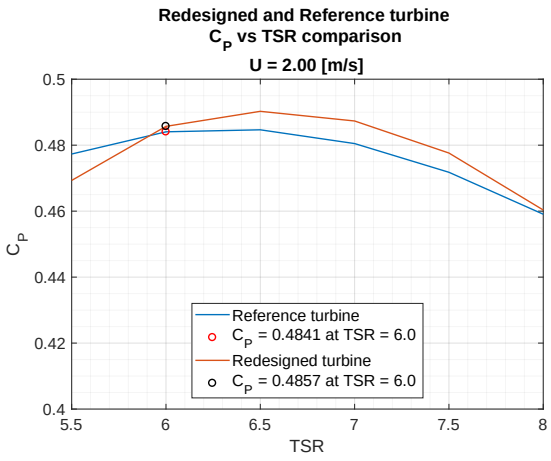

Figure 19: Redesigned and reference turbine C_P vs TSR comparison

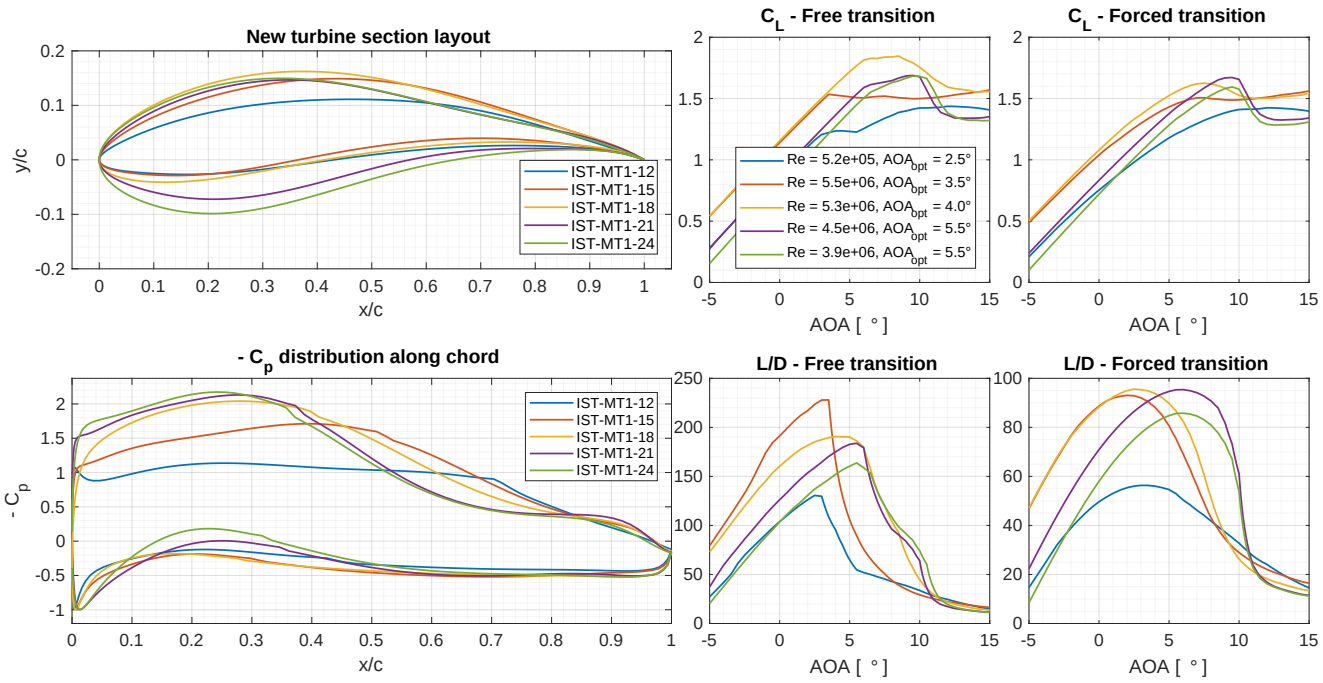

Figure 16: Chosen hydrofoils incorporating redesigned turbine blades

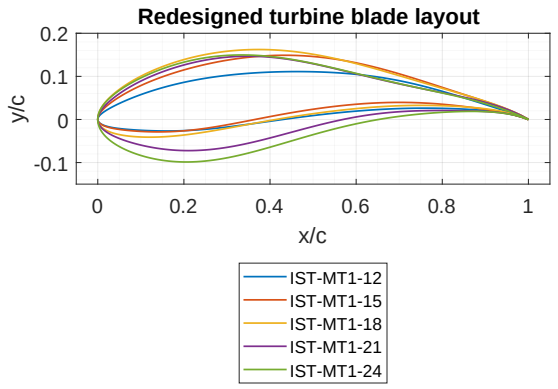

Figure 20: Blade section layout

Table 4: Redesigned turbine data

Span r/R [%]	Chord c/R [%]	Thickness t/c [%]	Pitch θ [°]	Chord reduction [%]
20	12.6	24.0	24.2	16.0
25	12.2	22.5	22.9	17.5
30	11.4	21.0	20.8	20.4
31	10.5	20.7	18.0	24.5
35	9.4	19.5	15.1	29.4
40	8.4	18.7	12.8	33.5
44	7.4	18.1	11.0	37.4
45	6.5	18.0	9.5	41.0
50	6.0	17.6	8.2	40.9
55	5.6	17.1	7.1	39.6
60	5.3	16.6	6.3	37.7
65	4.9	16.1	5.6	35.8
70	4.6	15.6	5.2	34.5
74	4.5	15.1	5.1	31.3
75	4.3	15.0	5.0	28.0
80	3.9	14.6	5.0	24.9
85	3.4	14.1	5.1	22.0
90	2.7	13.6	5.1	19.6
93	1.7	13.1	5.1	17.8
100	0.6	12.0	5.2	16.9

6. Conclusions

In this section, each topic is addressed individually and finally, future work recommendations are made.

Cost function evolution

Along this work the cost function evolved incrementally aiming to further and fully explore the design space.

CF2 is successful in increasing the cavitation margin for all sections. Cavitation margin values of up to 3 relative to the local cavitation number are obtained.

Regarding CF1, hydrofoils with good performance for a range of angles of attack around the optimum angle of attack are also obtained. The output Pareto front also features good spread, fully exploring the available design space. Additional optimizations for section $r/R \approx 100\%$ are carried to further increase performance and cavitation margin. Cost function EIGHT C outputs hydrofoils of maximum thickness of 12% with better performance than for version FIVE C, although not increasing cavitation margin.

Optimized hydrofoils' performance relative to reference hydrofoils

The optimized hydrofoils' display improvements in maximum L/D and optimum C_L of up to 66.10%

and 23.06%, respectively, in the clean regime; in the rough regime, improvements in maximum L/D and optimum C_L reach values of 73.21% and 99.82%, respectively, relative to the reference hydrofoils of the series NACA 63-8XX at the same cavitation margin. Regarding the reference hydrofoils of series NACA 66-8XX, improvements reach larger values. These results mean the optimized hydrofoils have better overall performance when considering a weighted balance of free and forced transition. This fact proves that the optimization setup is successful in improving on the performance of the reference hydrofoils on all fronts, meaning that, if transition occurs, the optimized hydrofoils will perform better than the reference foil sections.

Redesigned turbine with selected IST-MT1-XX foils

The criteria employed for hydrofoil selection consists on: hydrofoils of adjacent sections having equal or similar optimum angle of attack; high value of L/D, in order to obtain a greater energy conversion efficiency in turbine operation, i.e., higher C_P; similarity of the hydrofoil geometry along the radius of the blade r. This criteria results in the selection of hydrofoils IST-MT1-24, IST-MT1-21, IST-MT1-18, IST-MT1-15 and IST-MT1-12.

The reference turbine is successfully redesigned to incorporate the hydrofoils IST-MT-XX in its blades, yielding a power coefficient of C_P of 0.4857 at the design conditions of $TSR = 6$ and $U = 2$ m/s. This change in C_P represents an increase of 0.33%. For the off design conditions of $TSR = 6.5$, the increase in C_P is of 1.16%.

Lifting line theory predicts a significant chord reduction between the reference and redesigned turbines, which suggests that it would be possible to have the same power output while operating a turbine with smaller, lighter and thus cheaper blades.

Future Work

Regarding future work in the energy generation from marine currents field, more specifically through marine current turbines, there are several additional parameters and considerations that can be taken into account:

- Quantification of the importance that should be given to each transition regime: the amount of time that turbine blades operate with free or forced transition is unknown. In this work, equilibrium between clean and rough regimes is intended; however, there is uncertainty regarding which regime is more important;
- Further optimization of operation with forced transition: despite the previous point, if transition is to occur, the turbine performance is largely affected. Given the adverse environment in which these turbines operate and the likely possibility that the blades may become soiled in some manner, transition is likely to occur and thus a better performance with forced transition should be an aim of future studies;
- Comprehensive analysis of fouling effects: studying the influence of fouling and optimizing hydrofoils and blades to counter its adverse effects can, in the future, extend the range of operating conditions and prevent anomalous situations that could severely hinder the turbine operational performance;
- Include turbulent perturbations' influence: fluctuations induced by in-flow turbulence on the effective section velocity and angle of attack should be accounted for;
- Include wave influence: modelling the effects on flow speed and local pressure due to the presence of ocean waves can further prepare optimized hydrofoils for real operating conditions.

Acknowledgements

The author would like to thank Professor Ricardo Pereira, João Baltazar and Professor José Falcão de Campos for the support, dedication and remarkable professionalism given both as supervisors and teachers in the realization of this work.

References

[1] The Executive Committee of Ocean Energy Systems. An overview of Ocean Energy activities in 2017 - Annual Report. Technical report, 2017.

[2] Robin Pelc and Rod M. Fujita. Renewable energy from the ocean. *Marine Policy*, 26(6):471–479, 2002.

[3] Kai Wern Ng, Wei Haur Lam, and Khai Ching Ng. 2002-2012: 10 Years of Research Progress in Horizontal-Axis Marine Current Turbines. *Energies*, 6(3):1497–1526, 2013.

[4] M. J. Khan, G. Bhuyan, M. T. Iqbal, and J. E. Quaicoe. Hydrokinetic energy conversion systems and assessment of horizontal and vertical axis turbines for river and tidal applications: A technology status review. *Applied Energy*, 86(10):1823–1835, 2009.

[5] A. Roberts, B. Thomas, P. Sewell, Z. Khan, S. Balmain, and J. Gillman. Current tidal power technologies and their suitability for applications in coastal and marine areas. *Journal of Ocean Engineering and Marine Energy*, 2(2):227–245, 2016.

[6] Long Chen and Wei Haur Lam. A review of survivability and remedial actions of tidal current turbines. *Renewable and Sustainable Energy Reviews*, 43:891–900, 2014.

[7] Long Chen and Wei Haur Lam. Methods for predicting seabed scour around marine current turbine. *Renewable and Sustainable Energy Reviews*, 29:683–692, 2014.

[8] Leon Chernin and Dimitri V. Val. Probabilistic prediction of cavitation on rotor blades of tidal stream turbines. *Renewable Energy*, 113:688–696, 2017.

[9] Gael de Oliveira. *Wind Turbine Airfoils with Boundary Layer Suction - A Novel Design Approach*. PhD thesis, Delft University of Technology, Delft, the Netherlands, 2011.

[10] H. Ouyang, L. Weber, and A. J. Odgaard. Design optimization of a two-dimensional hydrofoil by applying a genetic algorithm. *Engineering Optimization*, 38(5):529–540, 2006.

[11] Jai N. Goundar, M. Rafiuddin Ahmed, and Young Ho Lee. Numerical and experimental studies on hydrofoils for marine current turbines. *Renewable Energy*, 42:173–179, 2011.

[12] Xing Qi Luo, Guo Jun Zhu, and Jian Jun Feng. Multi-point design optimization of hydrofoil for marine current turbine. *Journal of Hydrodynamics*, 26(5):807–817, 2014.

[13] Matthieu Sacher, Mathieu Durand, Élisa Berrini, Frédéric Hauville, Régis Duvigneau, Olivier Le Maître, and Jacques André Astolfi. Flexible hydrofoil optimization for the 35th America's Cup with constrained EGO method. *Ocean Engineering*, 157(September 2017):62–72, 2018.

[14] A. S. Bahaj, A. F. Molland, J. R. Chaplin, and W. M J Batten. Power and thrust measurements of marine current turbines under various hydrodynamic flow conditions in a cavitation tunnel and a towing tank. *Renewable Energy*, 32(3):407–426, 2007.

[15] J.A.C. Falcão de Campos. Hydrodynamic Power Optimization of a Horizontal Axis Marine Current Turbine with Lifting Line Theory. In *ISOPE*, pages 307–313. ISOPE, 2007.

[16] Mark Drela and Harold Youngren. XFOIL - Subsonic airfoil development system, 2013.

[17] J. Baltazar and J.A.C. Falcao de Campos. Hydrodynamic Analysis of a Horizontal Axis Marine Current Turbine With a Boundary Element Method. *Journal of Offshore Mechanics and Arctic Engineering*, 133(4):041304, 2011.

[18] Ricardo Balbino Dos Santos Pereira, Gael De Oliveira, W A Timmer, and E Quaeghebeur. Probabilistic Design of Airfoils for Horizontal Axis Wind Turbines. page 10, 2018.

[19] Tian-tian Zhang, Wei Huang, Zhen-guo Wang, and Li Yan. A study of airfoil parameterization, modeling, and optimization based on the computational fluid dynamics method. *Journal of Zhejiang University-SCIENCE A*, 17(8):632–645, 2016.

[20] Ricardo Balbino Dos Santos Pereira. *Active Stall Control of Horizontal Axis Wind Turbines - A dedicated study with emphasis on DBD plasma actuators*. PhD thesis, Delft University of Technology, 2017.

[21] R. P. J. O. M. van Rooij and W. A. Timmer. Roughness Sensitivity Considerations for Thick Rotor Blade Airfoils. *ASME 2003 Wind Energy Symposium*, 125(November):22–31, 2003.

[22] W. A. Timmer and R. P. J. O. M. van Rooij. Summary of the Delft University Wind Turbine Dedicated Airfoils. *Journal of Solar Energy Engineering*, 125(4):488, 2003.